Control of Magnetic Ordering by Jahn−Teller Distortions in Nd_2GaMnO_6 and La_2GaMnO_6

Edmund J. Cussen,[†] Matthew J. Rosseinsky,*[,†] Peter D. Battle,*[,‡] Jonathan C. Burley,[‡] Lauren E. Spring,[‡] Jaap F. Vente,[‡] Stephen J. Blundell,[§] Amalia I. Coldea,[§] and John Singleton[§]

Contribution from the Department of Chemistry, University of Liverpool, Liverpool L69 7ZD, U.K., Inorganic Chemistry Laboratory, University of Oxford, South Parks Road, Oxford OX1 3QR, U.K., and Clarendon Laboratory, Department of Physics, University of Oxford, Parks Road, Oxford OX1 3PU, U.K.

Received August 22, 2000

Abstract: The substitution of Ga^{3+} into the Jahn−Teller distorted, antiferromagnetic perovskites $LaMnO_3$ and $NdMnO_3$ strongly affects both the crystal structures and resulting magnetic ordering. In both compounds the Ga^{3+} and Mn^{3+} cations are disordered over the six coordinate sites. La_2GaMnO_6 is a ferromagnetic insulator ($T_c = 70$ K); a moment per Mn cation of 2.08(5) μ_B has been determined by neutron powder diffraction at 5 K. Bond length and displacement parameter data suggest Jahn−Teller distortions which are both coherent and incoherent with the *Pnma* space group symmetry of the perovskite structure ($a = 5.51122(4)$ Å, $b = 7.80515(6)$ Å, $c = 5.52947(4)$ Å) at room temperature. The coherent distortion is strongly suppressed in comparison with the parent $LaMnO_3$ phase, but the displacement ellipsoids suggest that incoherent distortions are significant and arise from local Jahn−Teller distortions. The preparation of the new phase Nd_2GaMnO_6 has been found to depend on sample cooling rates, with detailed characterization necessary to ensure phase separation has been avoided. This compound also adopts the $GdFeO_3$-type orthorhombically distorted perovskite structure (space group *Pnma*, $a = 5.64876(1)$ Å, $b = 7.65212(2)$ Å, $c = 5.41943(1)$ Å at room temperature). However, the B site substitution has a totally different effect on the Jahn−Teller distortion at the Mn^{3+} centers. This phase exhibits a Q_2 mode Jahn−Teller distortion similar to that observed in $LaMnO_3$, although reduced in magnitude as a result of the introduction of Ga^{3+} onto the B site. There is no evidence of a dynamic Jahn−Teller distortion. At 5 K a ferromagnetically ordered Nd^{3+} moment of 1.06(6) μ_B is aligned along the *y*-axis and a moment of 2.8(1) μ_B per Mn^{3+} is ordered in the *xy* plane making an angle of 29(2)° with the *y*-axis. The Mn^{3+} moments couple ferromagnetically in the *xz* plane. However, along the *y*-axis the moments couple ferromagnetically while the *x* components are coupled antiferromagnetically. This results in a canted antiferromagnetic arrangement in which the dominant exchange is ferromagnetic. Nd_2GaMnO_6 is paramagnetic above 40(5) K, with a paramagnetic moment and Weiss constant of 6.70(2) μ_B and 45.9(4) K, respectively. An ordered moment of 6.08(3) μ_B per Nd_2GaMnO_6 formula unit was measured by magnetometry at 5 K in an applied magnetic field of 5 T.

Introduction

The strong electron−electron and electron−phonon interactions characteristic of manganese oxides have been widely invoked as explanations of colossal magnetoresistance. Although attention has predominantly focused on double-exchange interactions mediated by itinerant holes introduced into the e_g orbitals by oxidation of $LaMnO_3$, the Jahn−Teller distortion driven by lifting the orbital degeneracy of the $t_{2g}^3e_g^1$ configuration of Mn^{3+} is a key component of both vibronic and magnetic exchange interactions. The magnetic and crystal structures of $LaMnO_3$ clearly show the important role played by Jahn−Teller distortions, coherently ordered between neighboring sites, in controlling the exchange interactions by determining the occupancy of the e_g-symmetry orbitals. The antiferrodistortive orbital ordering arising from the cooperative Jahn−Teller effect and the resulting superexchange between half-filled and empty orbitals produces an A-type magnetic structure in which ferromagnetic MnO_2 sheets are coupled antiferromagnetically.[1] Considerable attention[2] has been paid to the disruption of the A-type antiferromagnetic order and the suppression of the long-range order of the Jahn−Teller distortion by holes introduced into the e_g orbitals upon the introduction of Mn^{IV} centers. In this paper we examine the effect of 50% substitution of a d^{10} ion at the octahedral site and find the magnetic behavior strongly altered from the parent Mn^{III} phases, despite the formal Mn oxidation state remaining unchanged. The transport and magnetotransport properties of the phases indicate that the strong influence of this substitution on structure and physical properties occurs without the introduction of charge carriers. The chemical control of the magnetic ordering is thus purely via the influence of the electronically spherical d^{10} cation on the crystal structure, particularly local orbital ordering at the Mn^{III} sites.

Previous work has shown that La_2GaMnO_6 (or $LaGa_{0.5}Mn_{0.5}O_3$) is a ferromagnet with unit cell parameters consistent with a reduced Jahn−Teller distortion when compared with

[†] Department of Chemistry, University of Liverpool.
[‡] Inorganic Chemistry Laboratory, University of Oxford.
[§] Department of Physics, University of Oxford.

(1) Goodenough, J. B. *Magnetism and the Chemical Bond*; Interscience: New York, 1963.
(2) Radaelli, P. G.; Iannone, G.; Marezio, M.; Hwang, H. Y.; Cheong, S.-W.; Jorgensen, J. D.; Argyriou, D. N. *Phys. Rev. B* **1997**, *56*, 8265−8276.

10.1021/ja003139i CCC: $20.00
Published on Web 01/18/2001

$LaMnO_3$.[3] This has been suggested to be due to superexchange interactions between dynamically disordered Jahn−Teller Mn^{III} centers, where the electronic configuration (e_g orbital occupancy) at the Mn^{III} sites follows the vibrational motion, with the axis of the ferromagnetic interactions rotating rapidly with respect to the spin relaxation time as the direction of the Jahn−Teller distortion is dynamically exchanged between the local *x*, *y*, and *z* axes. A detailed understanding of the orbital ordering, both static and dynamic, requires knowledge of the average crystal structure and the atomic displacement parameters. Neutron diffraction is extremely sensitive to oxide anion positions and displacements, so here we present the crystal structure of this phase determined from neutron powder data at 300, 50, and 5 K. These data show the importance of the static Jahn−Teller distortions which are averaged to zero by the space group symmetry, as well as those coherent with *Pnma*, in determining the Mn environment and the resulting exchange interactions.

The new phase Nd_2GaMnO_6 (or $NdGa_{0.5}Mn_{0.5}O_3$), which does not behave as a simple modification of La_2GaMnO_6, demonstrates the sensitivity of these systems to apparently minor changes in chemical composition. The crystal structure reveals a larger coherent Jahn−Teller distortion which translates into quite different magnetic behavior, with both ferro- and antiferromagnetic exchange between the Mn^{III} centers evident from the 5 K magnetic structure. Both ordered and disordered Jahn−Teller distortions are thus shown to be important in controlling the coupling between the spin and orbital degrees of freedom in these localized electron Mn^{III} systems.

Experimental Section

Black, polycrystalline samples of Nd_2GaMnO_6 and La_2GaMnO_6 were synthesized by standard solid-state ceramic techniques. Stoichiometric amounts of high-purity, dried Nd_2O_3 (or La_2O_3), Ga_2O_3, and MnO_2 were accurately weighed out and intimately mixed in an agate mortar and pestle. In the case of Nd_2GaMnO_6 these reactants were fired in air at 800 °C for 36 h as a powder, then pelleted and fired at 1000 °C for 30 h, 1200 °C for 22 h, and 1250 °C for 58 h with regrinding and repressing between firings. After each firing the sample was cooled by removal from the furnace at the reaction temperature. The product, cooled by air-quenching from 1200 °C, formed at this stage will be referred to as sample **A**. Finally, sample **A** was heated at 1400 °C for 22 h as a pellet and quenched into liquid nitrogen to produce sample **B**. In the case of La_2GaMnO_6 the heating cycle was 36 h at 850 °C, 12 h at 1000 °C, 60 h at 1200 °C, and 48 h at 1300 °C.

X-ray powder diffraction patterns were collected in the angular range $10 < 2\theta/° < 120$ in steps of $\Delta 2\theta = 0.02°$ on a Siemens D5000 diffractometer in Bragg−Brentano geometry with Cu $K\alpha_1$ radiation. Synchrotron X-ray powder diffraction data were collected on La_2GaMnO_6 on station 2.3 at the Synchrotron Radiation Source, Daresbury Laboratory ($\lambda = 1.300$ Å, $15 \le 2\theta/° \le 100$, $\Delta 2\theta = 0.01°$). Neutron diffraction data were collected on the D2b powder diffractometer at the Institut Laue-Langevin, Grenoble ($\lambda = 1.5940$ Å). Data were collected on La_2GaMnO_6 at 290, 50, and 5 K ($8 \le 2\theta/° \le 150$, step size $\Delta 2\theta = 0.05°$) and on Nd_2GaMnO_6 at 5 K. Room temperature time-of-flight powder diffraction data were collected on Nd_2GaMnO_6 on the High-Resolution Powder Diffractometer (HRPD) at the ISIS spallation neutron source, Rutherford Appleton Laboratory.

Absorption corrections and normalization of the HRPD data were carried out using the GENIE software.[4] Rietveld refinement[5] of data from HRPD was carried out with the program TF12[6] incorporating subroutines from the Cambridge Crystallographic Library, and the data from D2b were analyzed with use of the GSAS[7] program suite.

Magnetic susceptibility measurements were performed in an applied field of 100 Oe over the temperature range $5 \le T/K \le 300$ using a Quantum Design MPMS SQUID magnetometer. Data were collected after both zero field cooling (ZFC) and field cooling (FC) of the sample. Magnetization was measured as a function of field in the range $-50 \le H/kOe \le 50$ at a range of temperatures after cooling the sample in a field of 50 kOe.

Magnetotransport data were collected on sintered bars, approximately $5 \times 2 \times 2$ mm in size. Standard four-probe geometry was used, with the direct current (≤ 50 μA) perpendicular to the field. Resistivity was measured as a function of temperature while cooling the material from room temperature to 4.2 K in zero field. Magnetoresistance isotherms were measured at fields between 0 and 14 T at 200, 150, and 114 K for La_2GaMnO_6 and 200 K for Nd_2GaMnO_6. During each field sweep, the temperature fluctuation was maintained at no more than ±1 K. The sweeps were carried out for the lowest temperature first and warming between temperatures was performed under zero field.

Determination of the oxidizing power of La_2GaMnO_6 by iodometric routes proved unsuccessful, but sample **B** of Nd_2GaMnO_6 yielded an oxygen excess of only 0.004, too small to be detected in refinements of the diffraction data.

Results

La_2GaMnO_6. (a) Room Temperature Structure. The room temperature powder X-ray and neutron diffraction patterns were refined simultaneously (Figure 1) to provide enhanced sensitivity to possible cation vacancies at both A and B sites, which dominate the defect chemistry of $LaMnO_3$.[8] Both patterns could be indexed in the *Pnma* space group, demonstrating long-range disordering of the B-site cations consistent with their similar ionic radii. The tendency toward B-cation ordering in double perovskites is greater when there is an appreciable (>2 units) charge difference between two cations and when their sizes differ by more than 0.10 Å. Neither of these criteria are satisfied by the Mn^{3+},Ga^{3+} pair, thus the absence of cation ordering is not surprising. No evidence for deviation from the ideal cation stoichiometry at either the A or B sites was found in the refinements. Structural parameters are given in Table 1, and important bond lengths and angles are given in Table 2. The MnO_6 displacement parameters are represented in Figure 4a.

(b) Magnetic Behavior. The variation of molar susceptibility with temperature in a 100 Oe field for La_2GaMnO_6 is shown in Figure 2a. The sample undergoes a magnetic transition at 70 K, obtained from the first derivative of susceptibility with respect to temperature. The value of T_C and the low-temperature behavior are similar to those observed by Töpfer and Goodenough.[3] The low-temperature behavior is characterized by a broad maximum in the ZFC signal, while the value of the FC signal continues to increase after the divergence between the two at 70 K. The data follow the Curie−Weiss law between 230 and 300 K, with a Weiss constant of +126.7(8) K and an effective moment of 5.64 μ_B, exceeding the spin-only value of 4.89 μ_B.

Figure 2b shows that the linear magnetization isotherm at 300 K is replaced by nonlinear behavior below 100 K. Finite width hysteresis loops are evident at 50 and 5 K (albeit minimal for 50 K), which are symmetrical about the origin. At 5 K, the magnetization is 3.4μ_B per Mn in a field of 20 kOe.

(c) Low-Temperature Neutron Diffraction. Neutron powder diffraction data collected at 50 and 5 K showed that the *Pnma*

(3) Töpfer, J.; Goodenough, J. B. *Eur. J. Solid State Chem.* **1997**, *34*, 467.

(4) David, W. I. F.; Johnson, M. W.; Knowles, K. J.; Moreton-Smith, C. M.; Crosbie, G. D.; Campbell, E. P.; Graham, S. P.; Lyall, J. S. RAL report Genie RAL-86-102, Rutherford-Appleton Laboratory, 1986.

(5) Rietveld, H. M. *Acta Crystallogr.* **1969**, *2*, 65.

(6) Brown, P. J.; Matthewman, J. C. RAL report RAL-87-110, Rutherford-Appleton Laboratory, 1987.

(7) Larson, A. C.; von-Dreele, R. B. General Structure Analysis System (GSAS), Los Alamos National Laboratories, 1990.

(8) van-Roosmalen, J. A. M.; Cordfunke, E. H. P. *J. Solid State Chem.* **1994**, *110*, 106.

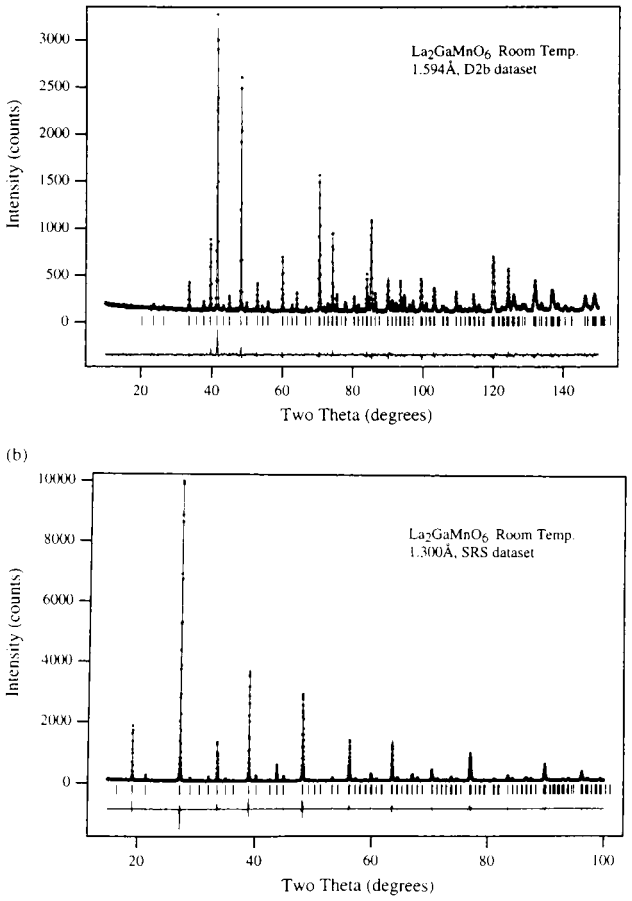

Figure 1. (a) Neutron and (b) X-ray Rietveld refinements of La_2GaMnO_6 at 300 K. The observed data are represented as points, the calculated fit as a line, and the difference curve is plotted below. The positions of the Bragg reflections are marked. Agreement indices are given in Table 1.

symmetry was maintained, with enhanced intensity in the low-angle reflections consistent with ferromagnetic long-range order. Refinement of a simple, single-sublattice ferromagnetic model accounted for the magnetic scattering with the spins orientated along the *y* direction ($m = 2.80(5)\ \mu_B$ per Mn at 5 K). The 5 K refinement is shown in Figure 3a with refined parameters and agreement indices in Table 1 and derived bond lengths in Table 2. The magnetic structure of La_2GaMnO_6 is shown in Figure 3b and the ORTEP diagram in Figure 4b.

(d) Magnetotransport Measurements. The magnetotransport behavior of La_2GaMnO_6 as a function of field at three selected temperatures is shown in Figure 5a. The observed ratio of negative magnetoresistance at 14 T in La_2GaMnO_6 increases on decreasing the measuring temperature, the signal being reduced to approximately 82% of its zero field value at 14 T and 114 K. The isotherm at 150 K has an approximately linear variation with field, and either side of it, the 200 and 114 K data, show "convex" and "concave" shaped curves, respectively. As shown in the inset of Figure 5a, the conductivity is thermally activated over the entire temperature range ($E_a = 0.20$ eV) in La_2GaMnO_6, and the insulating nature of the sample means resistivity is measurable only to 112 K. Application of a 14 T field at 5 K does not restore a measurable resistance ($\leq$300 MΩ).

Nd_2GaMnO_6. As will become clear, **B** is a highly crystalline sample of Nd_2GaMnO_6, whereas **A** is a sample of somewhat lower quality. In the account that follows we will describe briefly the characterization of sample **A** before presenting the detailed

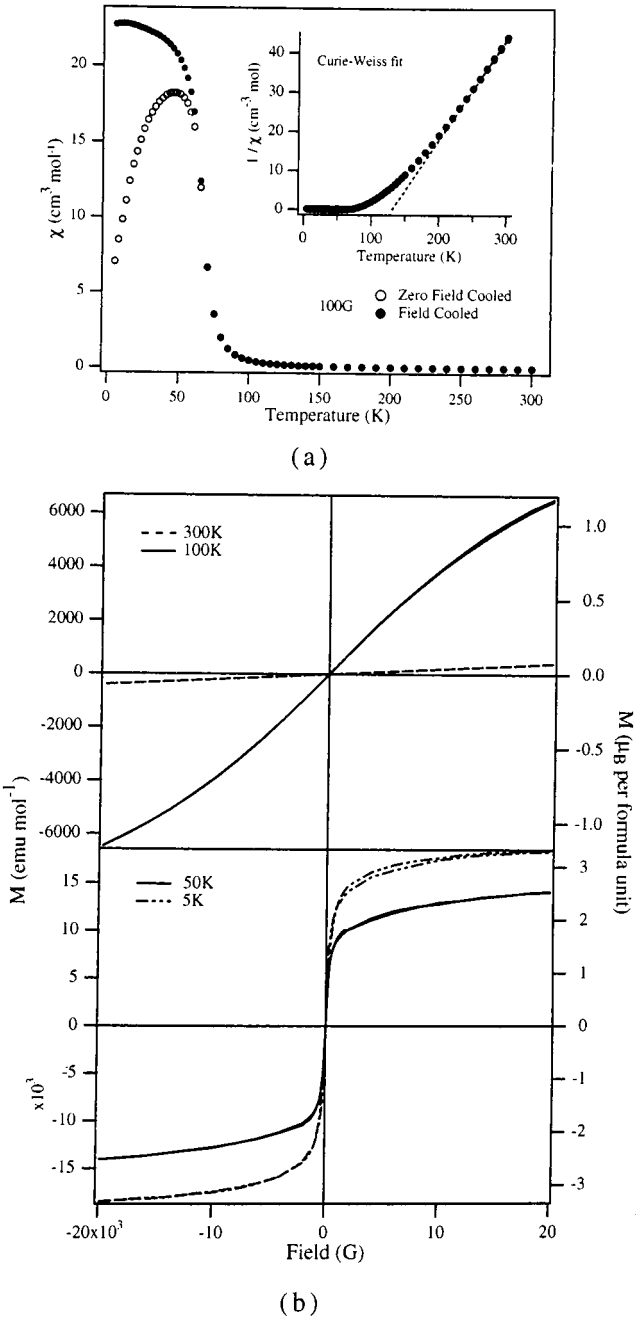

Figure 2. (a) M/H for La_2GaMnO_6 measured in a field of 100 Oe. The inset shows the Curie−Weiss plot over the entire temperature range. (b) Magnetization isotherms for La_2GaMnO_6 at 300, 100, 50, and 5 K.

description of the structural and electronic characteristics of sample **B**.

X-ray diffraction patterns recorded from sample **A** indicated that the *Pnma* space group was also adopted by this phase. The neutron diffraction data collected at room temperature contained no evidence of long-range cation ordering between Ga and Mn over the octahedrally coordinated sites, and trial refinements showed that the type of distortion was that previously reported for $Nd_{0.97}Mn_{0.95}O_3$[9] and $NdGaO_3$.[10] Nd_2GaMnO_6 therefore adopts the $GdFeO_3$ structure-type[11] containing corner linked Ga/MnO_6 octahedra which are tilted as shown in Figure 4.

(9) Cherepanov, V. A.; Barkatova, L. Y.; Petrov, A. N.; Voronin, V. I. *J. Solid State Chem.* **1995**, *118*, 53.
(10) Sanjuan, M. L.; Orera, V. M.; Merino, R. I.; Blasco, J. *J. Phys. Condens. Matter* **1998**, *10*, 11687.
(11) Geller, S. *J. Chem. Phys.* **1956**, *24*, 1236.

Table 1. Refined Parameters for La_2GaMnO_6 (5, 50, and 300 K) and Nd_2GaMnO_6 (5 and 300 K, sample **B**)[a]

	La_2GaMnO_6			Nd_2GaMnO_6	
	5 K	50 K	300 K	5 K	300 K
a (Å)	5.5098(1)	5.5115(1)	5.51122(4)	5.6426(1)	5.64577(1)
b (Å)	7.7961(2)	7.7986(2)	7.80515(6)	7.6340(1)	7.65213(2)
c (Å)	5.5220(1)	5.5238(1)	5.52947(4)	5.41129(9)	5.41943(1)
V (Å^3)	237.201(5)	237.428(6)	237.855(3)	233.10(1)	234.130(1)
Mn/Ga					
U_{iso} (Å^2)	0.0033(6)	0.0026(7)	0.0029(2)	0.0030(7)	0.0042(7)
M*y*/μ_B	2.80(5)	1.76(8)	0		
Ln					
x	0.5250(2)	0.5246(2)	0.5217(1)	0.5574(1)	0.5556(1)
z	−0.0045(4)	−0.0043(4)	−0.0049(2)	0.0118(2)	0.0118(1)
U_{iso} (Å^2)	0.0034(2)	0.0042(2)	0.0027(1)	0.0016(2)	0.0053(2)
O4					
x	0.2232(3)	0.2228(3)	0.2248(3)	0.3054(2)	0.3054(1)
y	−0.0351(2)	−0.0354(2)	−0.0349(2)	0.0433(1)	0.04367(8)
z	0.2754(2)	0.2752(3)	0.2745(3)	0.2114(2)	0.2125(1)
U_{11} (Å^2)	0.0128(8)	0.0136(9)	0.010(1)	0.0118(5)	0.0097(5)
U_{22} (Å^2)	0.0011(7)	0.0017(8)	0.0050(9)	0.0048(4)	0.0031(4)
U_{33} (Å^2)	0.0022(6)	0.0031(7)	0.0038(9)	0.0041(3)	0.0019(4)
U_{12} (Å^2)	0.0013(8)	0.0020(9)	0.0003(9)	0.0008(4)	0.0001(3)
U_{13} (Å^2)	−0.0022(6)	−0.0034(6)	−0.0021(8)	0.0010(4)	0.0002(3)
U_{23} (Å^2)	−0.0005(7)	0.0012(8)	−0.0023(9)	0.0001(4)	−0.0008(3)
U_{par} (Å^2)	0.0109(8)	0.0128(9)	0.00991(7)	0.0073(7)	0.0046(7)
U_{perp} (Å^2)	0.0026(2)	0.0028(2)	0.00449(3)	0.0067(7)	0.0050(8)
U_{equiv} (Å^2)	0.0054(4)	0.0062(4)	0.0063(4)	0.0069(7)	0.0049(8)
O5					
x	0.9909(5)	0.9915(5)	0.9919(6)	0.9804(2)	0.9813(2)
z	0.0712(4)	0.0702(4)	0.0699(5)	0.9158(2)	0.9147(2)
U_{11} (Å^2)	0.0244(23)	0.022(2)	0.016(2)	0.0078(6)	0.0107(6)
U_{22} (Å^2)	0.0033(14)	0.002(1)	0.006(1)	0.0043(5)	0.0027(6)
U_{33} (Å^2)	0.0006(9)	0.001(1)	0.004(1)	0.0038(6)	0.0030(5)
U_{13} (Å^2)	0.0031(8)	0.0043(9)	0.002(1)	0.0007(5)	−0.0014(4)
U_{par} (Å^2)	0.0031(3)	0.0022(3)	0.0063(7)	0.0043(8)	0.0027(5)
U_{perp} (Å^2)	0.013(1)	0.012(1)	0.010(1)	0.005(1)	0.007(1)
U_{equiv} (Å^2)	0.0095(9)	0.009(1)	0.009(1)	0.0053(9)	0.0055(9)

[a] All parameters are determined by refinement of neutron powder diffraction data collected on D2B except the 300 K La_2GaMnO_6 parameters (determined by refinement of powder neutron (D2B) and X-ray (station 2.3, Daresbury Synchrotron Radiation Source) data $R_{wp} = 7.64\%$, $R_p = 6.09\%$, DW-d = 1.068 and $\chi^2_{red} = 1.937$ for 52 variables.) and the 300 K Nd_2GaMnO_6 parameters determined by refinement of neutron powder diffraction data collected on HRPD. ($R_{wp} = 5.18\%$, $R_p = 4.45\%$, reduced $\chi^2 = 2.26$, for 38 variables.) Agreement indices for La_2GaMnO_6: 50 K, $R_{wp} = 6.88\%$, $R_p = 5.34\%$, DW-d = 0.952, and $\chi^2_{red} = 1.969$ for 38 variables; 5 K, $R_{wp} = 6.14\%$, $R_p = 4.71\%$, DW-d = 0.791 and $\chi^2_{red} = 2.462$ for 39 variables. Nd_2GaMnO_6: 5 K, $R_{wp} = 3.62\%$, $R_p = 2.80\%$, reduced $\chi^2 = 1.647$, DW-d = 1.104 for 47 variables. The atomic positions in the *Pnma* space group are the following: Mn/Ga, 4*b* 1 (0,0,0); Ln, O5, *m* (*x*,*1/4*,*z*); O4, *8d* 1 (*x*,*y*,*z*). Mn and Ga occupy the 4b site in a 1:1 ratio. The ferromagnetic moment refined at this site is quoted per Mn. The details of the refined magnetic structure for Nd_2GaMnO_6 at 5 K are given in the text.

Table 2. Bond Lengths (Å) and Angles (deg) in La_2GaMnO_6 (5, 50, 300 K) and Nd_2GaMnO_6 (5 and 300 K)

	La_2GaMnO_6			Nd_2GaMnO_6	
	5 K	50 K	300 K	5 K	300 K
Mn−O(4) × 2	1.975(1)	1.973(2)	1.978(2)	1.9377(9)	1.9350(8)
Mn−O(4) × 2	1.984(1)	1.987(2)	1.982(2)	2.0944(9)	2.1011(8)
Mn−O(5) × 2	1.9890(5)	1.9878(5)	1.9898(6)	1.9653(3)	1.9703(2)
Mn−O(4)−Mn	160.15(8)	159.98(9)	160.5(1)	151.59(5)	151.60(4)
Mn− O(5)−Mn	157.0(1)	157.3(1)	157.4(1)	152.39(7)	152.30(6)
O(4)−Mn−O(4)	88.75(1)	88.71(1)	88.71(2)	90.05(1)	90.18(1)
O(4)−Mn−O(5)	89.5(1)	89.8(1)	89.7(1)	90.61(4)	90.60(3)
O(4)−Mn −O(5)	89.9(1)	89.8(1)	89.9(1)	88.88(4)	89.00(3)
Ln−O(4) × 2	2.639(2)	2.640(2)	2.643(2)	2.383(1)	2.3814(9)
Ln−O(4) × 2	2.780(1)	2.783(2)	2.797(2)	2.587(1)	2.592(1)
Ln−O(4) × 2	3.177(1)	3.178(2)	3.164(1)	2.6593(9)	2.6720(8)
Ln−O(4) × 2	2.480(2)	2.476(2)	2.479(1)	3.442(1)	3.4408(8)
Ln−O(5)	2.600(2)	2.605(3)	2.623(3)	2.354(1)	2.341(1)
Ln−O(5)	2.972(2)	2.965(3)	2.949(3)	2.442(1)	2.459(1)
Ln−O(5)	2.399(3)	2.404(3)	2.411(3)	3.128(1)	3.135(1)
Ln−O(5)	3.135(3)	3.130(4)	3.128(3)	3.297(2)	3.285(1)

The crystallographic model described above was used to fit the data collected using D2b at 5 K and showed that the material does not undergo a structural phase transition on cooling from room temperature. However, the pattern contained additional Bragg peaks at low angle suggesting the presence of long-range magnetic order. The magnetic structure which best fitted these peaks was the same as that employed in the analysis of the data collected from sample **B**, as will be discussed later.

The fit parameters from sample **A** with these structural and magnetic models ($R_{wp} = 5.37$, $R_p = 4.10$, and $\chi^2 = 4.19$ for 46 variables) were acceptable, but we were not satisfied with the appearance of the difference curve and so experimented with

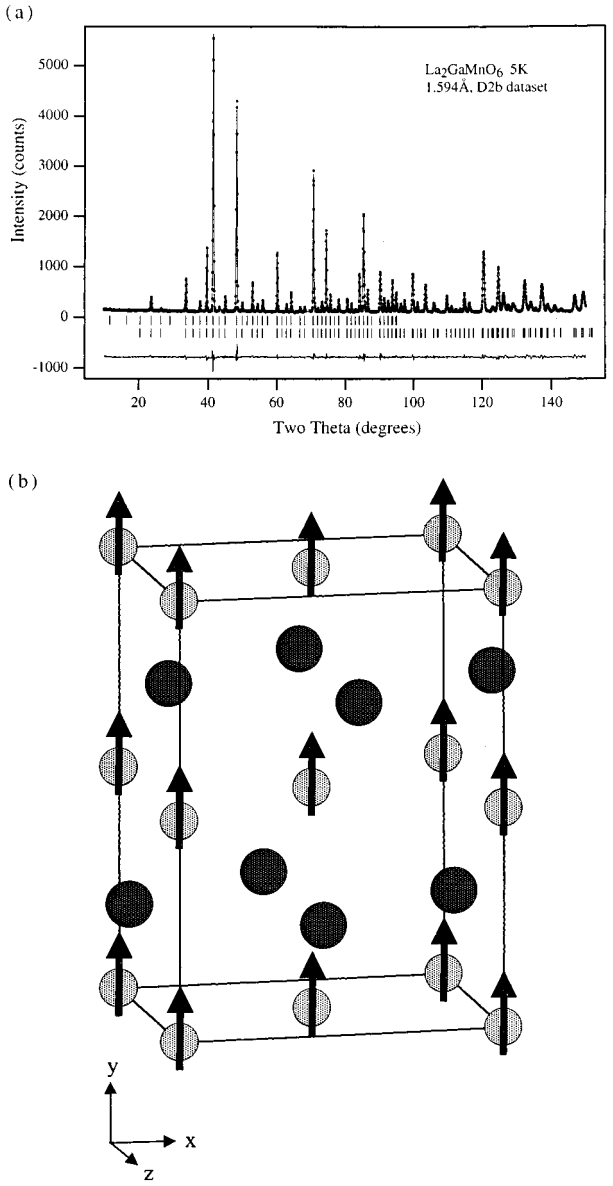

Figure 3. (a) Rietveld refinement of neutron powder diffraction data from ferromagnetically ordered La_2GaMnO_6 at 5 K. The data are represented as in Figure 1: the upper set of tick marks correspond to the magnetic phase. (b) Magnetic structure of La_2GaMnO_6 at 50 K, with the spin directions of Mn cations shown. Mn cations have 50% occupancy of the B-cation sites.

introducing a second perovskite phase of the same symmetry into the refinement. We have previously observed that samples of the $n = 2$ Ruddlesden−Popper compounds $Sr_{2-x}Nd_{1+x}Mn_2O_7$ could not be described by a single-phase model but required the use of two structurally similar phases to fit the neutron diffraction data.[12] We were thus highly cautious in the characterization of the present compound and alarmed by the improvement in the quality of fit ($R_{wp} = 4.75$, $R_p = 3.75$, and $\chi^2 = 3.39$) which was achieved by describing sample **A** as biphasic. Reanalysis of the laboratory X-ray data revealed that the 200 reflections had an asymmetric peak shape as shown in Figure 6. There were no other *h*00 reflections of appreciable intensity in the pattern. This asymmetry, when considered in conjunction with the improvement in the fit to the neutron data obtained by using a two-phase model suggested that the microtexture of the

(12) Battle, P. D.; Green, M. A.; Laskey, N. S.; Millburn, J. E.; Radaelli, P. G.; Rosseinsky, M. J.; Sullivan, S. P.; Vente, J. F. *Phys. Rev. B* **1996**, *54*, 15967.

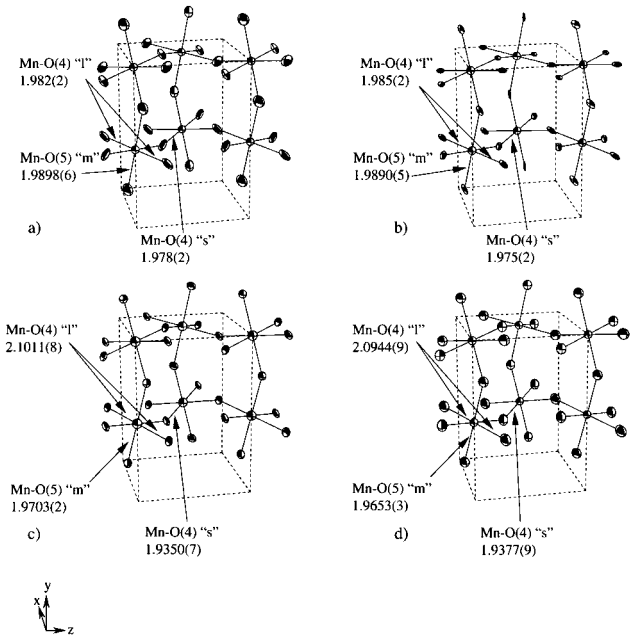

Figure 4. ORTEP plot of the MnO_6 octahedra in La_2GaMnO_6 at (a) 300 K and (b) 5 K and in Nd_2GaMnO_6 at (c) 300 K and (d) 5 K. The ellipsoids are drawn at the 99% probability level.

material disallows a monophasic description of this sample. Single and two phase refinements of sample **A** of Nd_2GaMnO_6 are given in Figure S1.

To probe the problem of sample homogeneity, various heat treatments were performed on sample **A**. Heating the sample at 1400 °C and air cooling gave little improvement in the quality of the sample, as evaluated by X-ray diffraction. However, as shown in Figure 6 quenching the sample from this temperature into liquid N_2 resulted in an asymmetry reduction and a relative narrowing of the 200 reflection in the X-ray diffraction pattern, thus indicating that the homogeneity and crystallinity of the material had been increased. The resulting product, sample **B**, was then thoroughly evaluated using neutron diffraction.

Data were collected at room temperature with the HRPD instrument and could be satisfactorily fitted by using the structural model based on the $GdFeO_3$ structure described above. The Rietveld refinement utilized a total of 36 variables including 3 lattice parameters, 7 atomic positional parameters, 2 isotropic metal temperature factors, and 10 anisotropic temperature factors which described the thermal motion of the oxide ions. Several regions of the diffraction pattern were excluded from the refinement due to the presence of reflections from the vanadium can. The fit obtained to the data using this model is shown in Figure 7. The atomic parameters and bond lengths and angles resulting from this structural refinement are given in Tables 1 and 2, respectively. It is interesting to note that the Bragg reflections from this material were sufficiently sharp that it was necessary to employ the peakshape function contained within the TF12 code[6] in order to fit the data satisfactorily; inferior refinements resulted when GSAS was used.

The diffractometer D2b was used to characterize the sample at 5 K and yielded data similar to those collected from sample **A**; no structural transition was evident on cooling the sample and additional Bragg peaks were observed at low angle. The high angle data were fitted by using a crystallographic model based on the observed room temperature structure. The difference plot obtained from this structural fit to the pattern clearly showed that, as well as several peaks at low angle which are disallowed in space group in *Pnma* (no cell enlargement is

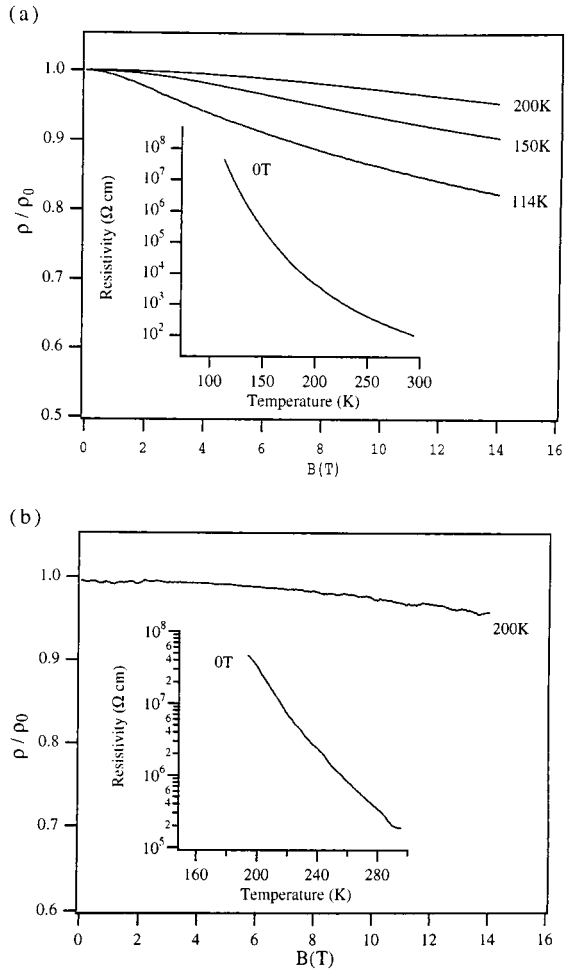

Figure 5. Field dependence of the normalized resistivity $\rho(B)/\rho(0)$ (a) at 200, 150, and 114 K for La_2GaMnO_6 and (b) at 200 K for Nd_2GaMnO_6. The insets show the temperature dependence of the resistivity at zero field.

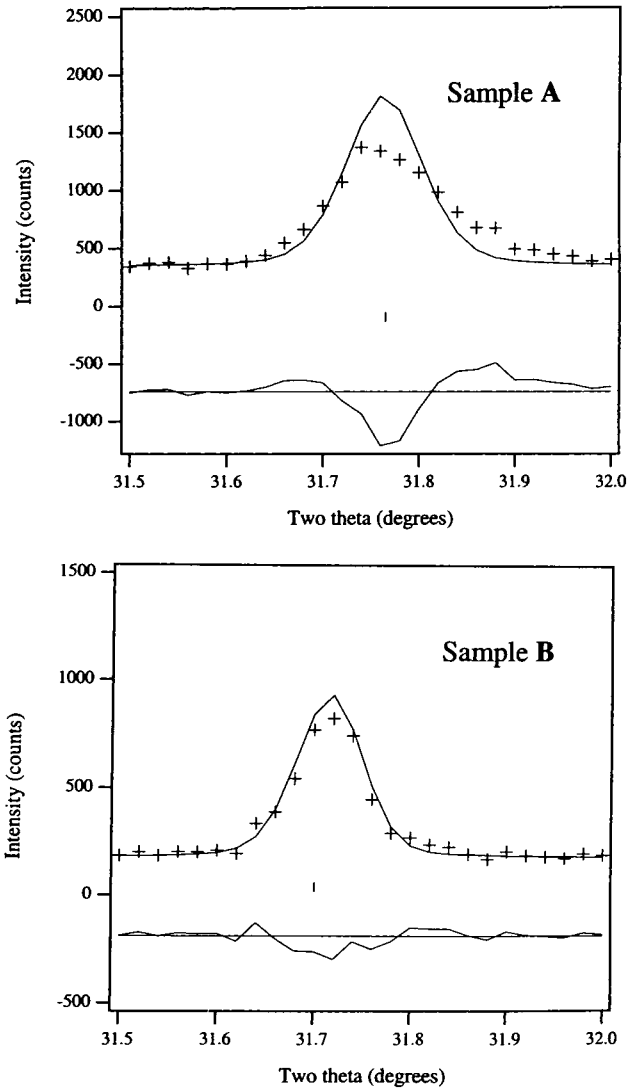

Figure 6. X-ray diffraction data collected from samples **A** (top) and **B (**bottom) of Nd_2GaMnO_6 containing the 200 reflections. The observed data (crosses) were fitted by a pseudo-Voigt function (line).

required to account for these reflections), there was a magnetic contribution to several of the allowed nuclear peaks. The former observation is indicative of the presence of an antiferromagnetic component to the magnetic structure while the latter requires at least partial ferromagnetic order in any proposed magnetic model. It was therefore necessary to employ the systematic approach of group theory. The moments on both Mn^{3+} and Nd^{3+} were refined within the constraints imposed by the symmetry relations of the 8 different allowed models.[13] The data could only be satisfactorily fitted by a ferromagnetic moment on Nd^{3+} oriented in the *y*-direction and with the moments on Mn having a ferromagnetically ordered component along *y* and G- and A-type antiferromagnetic components along *z* and *x*, respectively. This magnetic structure corresponds to the Γ_4[13] representation in Bertaut's macroscopic theory. The *z* component of the Mn moment refined to zero and so was subsequently fixed at this value. The refinement proceeded satisfactorily to convergence giving values of 1.06(6) μ_B for the ferromagnetic moment of Nd along *y* and 1.35(4) and 2.4(1) μ_B for the antiferromagnetic and ferromagnetic components of the Mn moment aligned along *x* and *y*, respectively, as shown in Figure 8. The Mn moment of 2.8(1) μ_B in the *xy* plane makes an angle of 29(2)° with the *y*-axis. The observed, calculated, and difference diffraction patterns are also shown in Figure 8 and the resulting atomic parameters and associated bond lengths and angles are given in Tables 1 and 2, respectively. ORTEP diagrams illustrating the thermal parameters Nd_2GaMnO_6 at 300 and 5 K are given in Figure 4.

(a) Magnetization Measurements. The temperature dependence of the magnetic susceptibility for sample **B** is shown in Figure 9. The data were fitted to the Curie−Weiss law, with an additional temperature independent parameter (TIP), in the temperature range $175 \leq T/K \leq 300$, giving values for the Curie constant, *C*, of 5.61(3) cm^3 K mol^{-1}, the Weiss constant, θ, of +45.9(4) K, and the TIP of 8.9(8) $\times$ 10^{-4} cm^3 mol^{-1}. The magnitude of the susceptibility increases sharply below 40(5) K and shows divergence below 21(1) K between the field-cooled and zero-field-cooled values. The latter passes through a maximum value at 14(1) K. The first derivative of the FC susceptibility with respect to temperature (Figure 9b) shows features at 14 and 10K which, given the complex nature of the magnetic ordering revealed by the refinement at 5 K, may correspond to the onset of order on the Nd sublattice or modification of the ordering motif on the Mn sublattice.

The magnetization of the sample as a function of field was recorded at several temperatures. As shown in Figure 9c, the magnetization is not saturated in a field of 50 kOe at 5 K reaching a maximum value of 6.08 μ_B per formula unit and a remanent magnetization of 1.53 μ_B.

(13) Bertaut, E. F.; Mareschal, J. *Solid State Commun.* **1967**, *5*, 93.

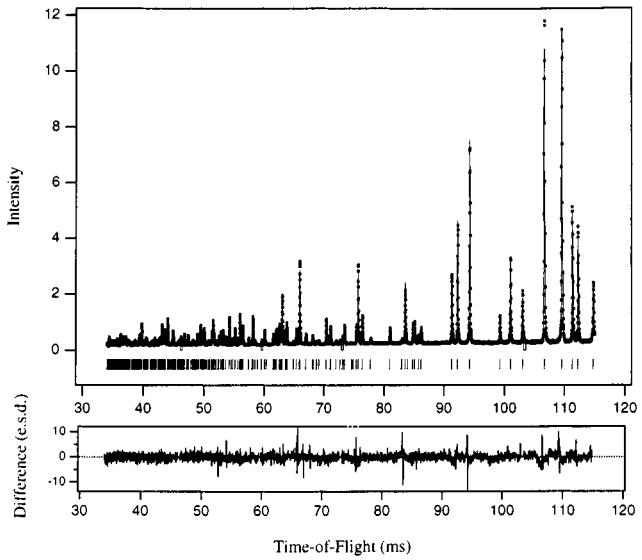

Figure 7. Observed (dots), calculated (line), and difference (represented as the difference of each point divided by the standard deviation of that point) time-of-flight neutron diffraction pattern collected from sample **B** of Nd_2GaMnO_6 at room temperature.

(b) Magnetotransport Measurement. The field and temperature dependence of the resistivity of Nd_2GaMnO_6 is shown in Figure 5b**.** The resistivity is thermally activated ($E_a = 0.271(4)$ eV) and the magnetoresistance is only −4% in a field of 14 T at 200 K. At all temperatures below 200 K the absolute value of the resistance was immeasurably large in fields of both 0 and 14 T.

Discussion

Our high-resolution neutron diffraction experiments show that Nd_2GaMnO_6 (sample B) and La_2GaMnO_6 both exhibit a $GdFeO_3$-like distortion of the perovskite structure. Orthorhombic perovskites have been separated into type O ($b/c > \sqrt{2}$), wherein the predominant distortion is octahedral tilting as in $GdFeO_3$, and type O′ ($b/c < \sqrt{2}$), wherein the predominant distortion is driven by the Jahn−Teller effect, as in $LaMnO_3$. The limitations of this approach, and of all where precise structural data are not available, are illustrated by $LaGaO_3$,[14] which has O′ cell parameters despite not containing a Jahn−Teller active cation. Both Nd_2GaMnO_6 and La_2GaMnO_6 are O′ according to this classification, but it is important to note that the orthorhombic strain $2(a - c)/(a + c)$ is an order of magnitude smaller in La_2GaMnO_6 compared with the $LnMnO_3$ parent phases, while the strain in Nd_2GaMnO_6 is larger than that found in $LaMnO_3$ and 56% of that in $NdMnO_3$. The strain in $NdGaO_3$ is more than twice that in $LaGaO_3$.

In both Nd_2GaMnO_6 and La_2GaMnO_6 the internal angles in the BO_6 octahedra do not deviate from 90° by more than 1.25°. These units rotate cooperatively about the ⟨110⟩ directions of the primitive cubic unit cell to adjust the A−O bond lengths and A coordination number. The smaller Nd^{3+} cation has a smaller first coordination sphere (8 anions within 2.673 Å with the secondary coordination sphere beginning at 3.1364 Å, La^{3+} 9 anions within 2.973 Å) and produces more significant octahedral tilting, with the Mn−O(4)−Mn and Mn−O(5)−Mn angles being respectively 9° and 5° greater. The tilt angle ($\sqrt{48}$ arctan(y(O4))[15] of 13.85(8)° in La_2GaMnO_6 is less than

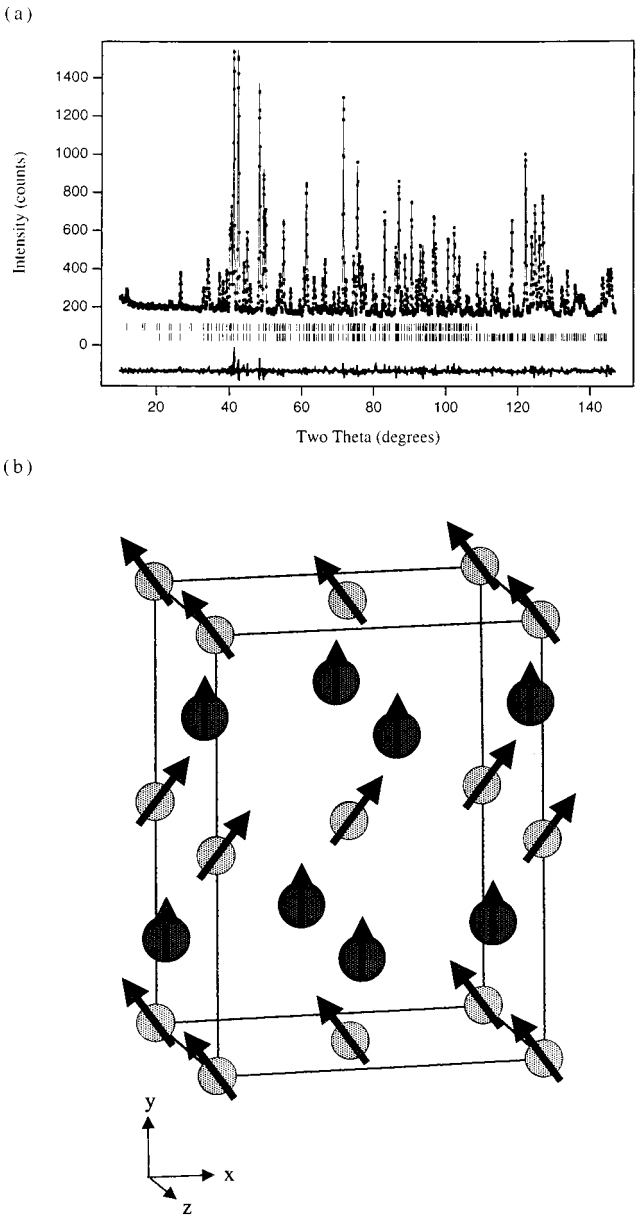

Figure 8. (a) Observed (dots), calculated (line), and difference neutron diffraction pattern of Nd_2GaMnO_6 collected at 5 K. Tick marks indicate reflections allowed by the symmetry of the nuclear cell. The upper reflection markers indicate the positions of allowed magnetic reflections. (b) The magnetic structure of Nd_2GaMnO_6 at 5 K. The moments on the Mn cations (small circles) are canted in the *xy* plane while those on the Nd cations (large circles) are directed along *y*. The Mn cation moment is 2.7(1)μ_B ($m_x = 1.36(4)$ μ_B, $m_y = 2.4(1)$ μ_B) and the Nd moment is 1.06(6) μ_B directed along *y*. The *x*-component of the Mn moment adopts the A-type arrangement while the *y*-component is ferromagnetically aligned.

that in $LaMnO_3$ (15.24(8)°) whereas the extent of tilting is comparable in $NdMnO_3$ (17.9(1)°)[16] and Nd_2GaMnO_6 (17.33(4)°). The rigidity of the BO_6 units allows the Mn−O distances to be used directly in computing the extent of distortion along the Jahn−Teller normal coordinates.

The mean B−O distances in the Ga-substituted phases are close to those expected from the simple mean values of these distances in the end members. Given the important role of cooperative Jahn−Teller distortions in controlling the magnetic

(14) Marti, W.; Fischer, P.; Altorfer, F.; Scheel, H. J.; Tadin, M. *J. Phys. Cond. Matter* **1994**, *6*, 127.

(15) O'Keefe, M.; Hyde, B. G. *Acta Crystallogr.* **1977**, *33*, 3802.

(16) Alonso, J. A.; Martinez-Lope, M. J.; Casais, M. T.; Fernandez-Diaz, M. T. *Inorg. Chem.* **2000**, *39*, 917−923.

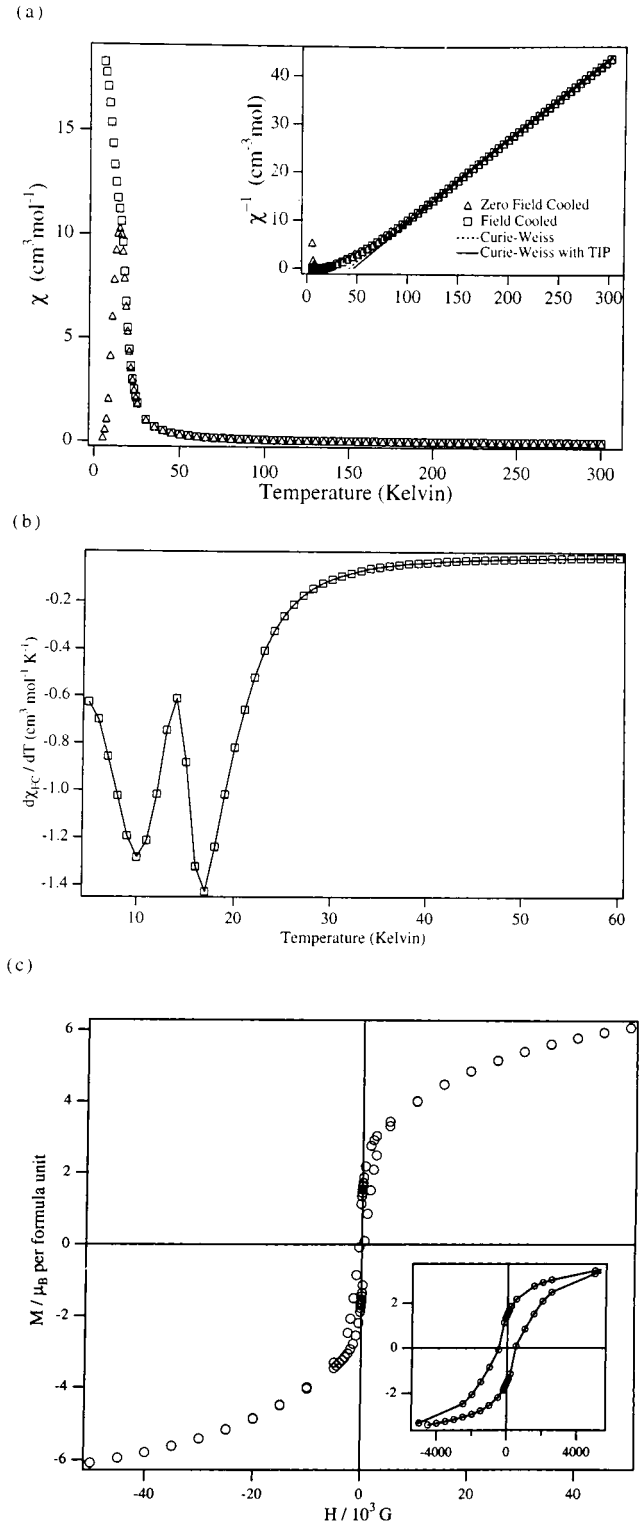

Figure 9. (a) The magnetic susceptibility of Nd_2GaMnO_6 (sample **B**) as a function of temperature in a field of 100 Oe. The inverse susceptibility data were fitted to the Curie−Weiss law between 175 and 300 K as shown by the solid line in the inset. (b) First temperature derivative of the field-cooled magnetic susceptibility of Nd_2GaMnO_6 (sample **B**). (c) The magnetization of Nd_2GaMnO_6 (sample **B**) as a function of field recorded at 5 K. The inset shows data around the origin.

structure of $LaMnO_3$, any attempt to explain the different magnetic behavior of the Ga-substituted phases must begin with an analysis of the implications of the observed bond lengths and atomic displacement parameters for the extent and long-range order of such distortions in the present phases. There are several quantities which may be computed to measure the extent of Jahn−Teller distortion at a particular site. σ_{JT} measures the deviation of the Mn−O bonds from the mean value.

$$\sigma_{JT} = \sqrt{{}^1/_6\sum_i[(B{-}O)_i - \langle B{-}O\rangle]^2}$$

where the summation is performed over each of the six Mn−O distances and $\langle B{-}O\rangle$ is the mean bond length on the octahedral site. The value of σ_{JT} observed for the 50% Ga phases may be compared with an expected value generated by averaging equivalent bonds in the $LnMnO_3$ and $LnGaO_3$ parent phases. The 300 K σ_{JT} value of 0.0709(4) for Nd_2GaMnO_6 is close to the expected value of 0.073, whereas in La_2GaMnO_6 σ_{JT} of 0.0048(7) is an order of magnitude less than the predicted value of 0.059. It is important to note that $NdGaO_3$ ($\sigma_{JT} = 0.0080$) is more distorted than $LaGaO_3$ ($\sigma_{JT} = 0.0047$). These parameters show a much larger static Jahn−Teller distortion coherent with the symmetry operators of *Pnma* in the case of Nd_2GaMnO_6 than in that of La_2GaMnO_6.

However, the small value of σ_{JT} for La_2GaMnO_6 is not necessarily consistent with the local and long-range distortions in La_2GaMnO_6 being small. The Jahn−Teller distortions at each Mn^{III} center could be extremely significant but average to zero upon application of the *Pnma* symmetry operators. This is the case in $La_{0.5}Ca_{0.5}MnO_3$,[2] which has well-defined Jahn−Teller distortions at the Mn^{3+} sites in the charge-ordered supercell, but refinement in the *Pnma* subcell gives no detectable coherent distortion. The signature of the incoherent Jahn−Teller distortions in $La_{0.5}Ca_{0.5}MnO_3$ is in the size of the displacement ellipsoids of the oxide anions, which at 0.01 Å^2 are greater than 0.003 Å^2 found in $LaMnO_3$ at 2 K. Diffraction-based structure refinements are only sensitive to such incoherent distortions, which may be static or dynamic, through the anisotropic displacement parameters, which contain information about the size and direction of atomic displacements from the average positions in *Pnma* symmetry. These parameters are particularly important as superexchange between orbitals whose occupancy is modulated by vibronic coupling to dynamic Jahn−Teller distortions has been put forward as an explanation for the ferromagnetism of La_2GaMnO_6.[3] The suppression of the coherent static Jahn−Teller distortion as shown by the B−O bond lengths indicates that the origin of the difference in magnetic behavior compared to $LaMnO_3$ does indeed lie in the large changes in Jahn−Teller distortions induced by B site substitution.

The Jahn−Teller distortion in $LaMnO_3$ can be analyzed in terms of two modes.[17] There are three different bonds, with the medium length Mn−O5 bond (m) directed along the *z* axis and long (l) and short (s) Mn−O4 bonds alternating along the *x* and *y* axes (Figure 10). Here *x*, *y*, and *z* are local axes at the Mn site oriented along the *a*, *c*, and *b* directions of *Pnma*. One Jahn−Teller mode is a ferrodistortive pseudotetragonal octahedral elongation, described by the normal mode $Q_1 = 2/\sqrt{6}$ (2m−l−s) which couples to the difference in electronic density between the e_g orbitals directed along the *z*-axis and those in the *xy* plane (Figure 10a). In $LaMnO_3$ this mode is negative as the m bond is shorter than the mean *xy* plane bond distance. The second mode $Q_2 = \sqrt{2}$ (l−s) is antiferrodistortive within the *xy* plane (Figure 10b), resulting in alternate long (l) and

(17) Kanamori, J. *J. Appl. Phys.* **1960**, *31*, 14S.

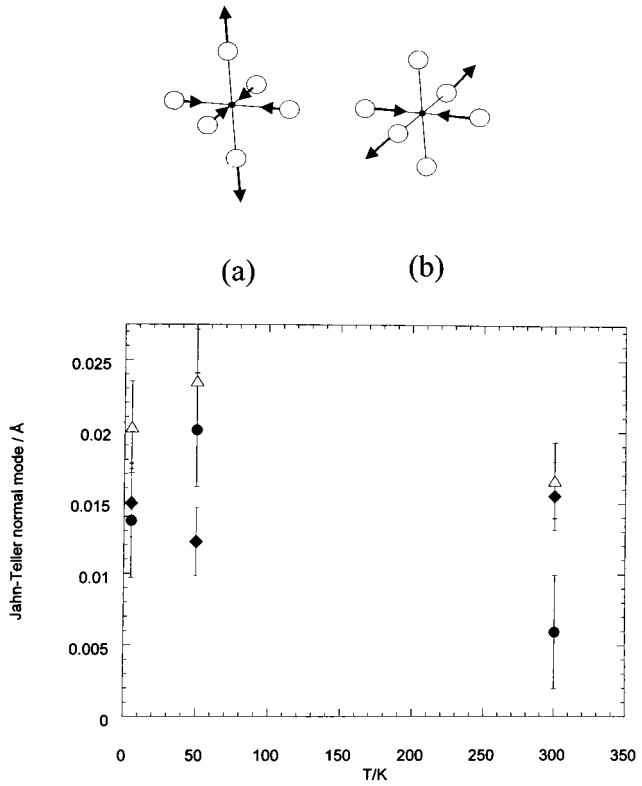

Figure 10. (a) Q_1 and (b) Q_2 Jahn−Teller distortions of the MnO_6 octahedra in *Pnma* symmetry perovskites, and the temperature dependence of the Jahn−Teller parameters Q_1 (diamonds) and Q_2 (circles) and $(Q_1^2 + Q_2^2)^{1/2}$ (open triangles) in La_2GaMnO_6. Note the maximum in Q_2 below the Curie temperature of 70 K. At 300 K in $LaMnO_3$, $Q_1 = -0.121$, $Q_2 = 0.383$, and $(Q_1^2 + Q_2^2)^{1/2} = 0.401$

short (s) Mn−O bonds within the plane. This mixes the x^2-y^2 and $3z^2-r^2$ e_g orbitals and produces a two-sublattice orbital ordering pattern, with a lower energy orbital $|a\rangle = c_1|x^2-y^2\rangle \pm c_2|3z^2-r^2\rangle$ and a higher energy orbital $|b\rangle = c_2|x^2-y^2\rangle \mp c_1|3z^2-r^2\rangle$ ($\pm$ referring to the two sublattices created by the antiferrodistortive Q_2 mode). The energy splitting of the e_g orbitals originally degenerate in octahedral symmetry is given by $E_{JT} = 2g\sqrt{Q_1^2+Q_2^2}$ and is estimated to be between 0.25 and 0.5 eV.[18] The coefficients c_1 and c_2 are given by the relations $\tan\phi = Q_2/Q_1$ and $\tan(\phi/2) = c_1/c_2$. In $LaMnO_3$ itself at 298 K $Q_2/Q_1 = -3.15$ [19] with the occupied $|a\rangle$ orbitals at the sublattice where the short Mn−O bond is directed along the *y*-axis being $|a\rangle \approx |z^2-x^2\rangle$ overlapping with empty $|b\rangle \approx |x^2-z^2\rangle$ orbitals on their immediate Mn neighbors which belong to the second sublattice. This results in ferromagnetic exchange within the plane as the electron occupying the $|a\rangle$ orbital on one site undergoes virtual transfer to the vacant $|b\rangle$ orbital at its neighbor, coupling ferromagnetically with both the electron in the neighboring $|a\rangle$ orbital and the t_{2g}^3 π electrons.

In contrast to the dominant Q_2 distortion in $LaMnO_3$, at 300 K in La_2GaMnO_6 the Mn−O(4) bonds within the *xy* plane are equal within experimental error, so $Q_2 = 0.006(4)$ is only significant to one standard deviation. The longest bond is Mn−O(5) directed along the crystallographic *b*-axis, giving a positive Q_1 ferrodistortive elongation ($Q_1 = 0.0155(2)$). This would be expected to stabilize the $3z^2-r^2$ orbital preferentially at each site and produce antiferromagnetic exchange, although the size of the static coherent contribution to E_{JT} is only 3.8% of that in $LaMnO_3$.

The temperature dependence of the bond lengths (Table 2) is evidence for significant electronic reorganization within La_2GaMnO_6 on cooling. The temperature dependence of the derived static coherent Jahn−Teller parameters (Q_n) in La_2GaMnO_6 is shown in Figure 10. On cooling below the Curie temperature of 70 K, structure refinements in the ferromagnetically ordered phase at 50 K reveal the onset of a small but significant Q_2 distortion, while Q_1 remains approximately independent of temperature. In view of the role of the Q_2 mode in generating the locally orthogonal orbital ordering responsible for the ferromagnetic sheets in $LaMnO_3$, the development of this nonzero static distortion below the magnetic ordering temperature may be important. Q_2/Q_1 is 1.6(4) at 50 K and 0.9(3) at 5 K, mixing in considerable $|x^2-y^2\rangle$ character to the $|a>$ orbital, which closely resembles $|z^2-y^2\rangle$ at 50 K. However, the static coherent contribution to E_{JT} never exceeds 5.8% of the value in $LaMnO_3$.

The static coherent distortions revealed by the bond lengths in La_2GaMnO_6 are small, yet the driving force for Jahn−Teller distortion at each Mn^{III} site is similar in size to that in $LaMnO_3$, with only the elastic cooperative coupling to neighboring Mn^{III} sites being diminished by the substitution of non-Jahn−Teller Ga^{3+} cations. The size of dynamically and statically disordered distortions represented by the anisotropic displacment ellipsoids must therefore be seriously considered. Inspection of the ellipsoids (Figure 4a,b) shows that their shape is inconsistent with interpretation in terms of conventional dynamic bond stretching and bending and is not significantly altered on cooling. The ellipsoid shapes differ drastically from those in Nd_2GaMnO_6 (Figure 4c,d), which are to first-order spherical, suggesting that incoherent distortions are of greater importance in the La phase. The rms displacements in La_2GaMnO_6 as measured by the equivalent isotropic temperature factors of the O(4) and O(5) oxide anions are insensitive to temperature, suggesting that incoherent static rather than dynamic Jahn−Teller effects are dominant. If a dynamic Jahn−Teller effect were operative at both 5 and 300 K, the barrier between equivalent Jahn−Teller minima would have to be less than 10 K.[20] This value is unreasonably low and a description in terms of static incoherent distortions in the magnetically ordered phase is therefore preferred. These static displacements would be expected to manifest themselves as enlargements of the U_{ij} ellipsoids along the B−O directions. The U_{ij} ellipsoids can be resolved into their components parallel and perpendicular to the B−O directions, with the results shown in Figure 11. Typically, in structural chemistry, the perpendicular component of the displacement ellipsoid is largest due to the enhanced ease of bond-bending over bond-stretching, so the observation that the reverse is true for the O4 oxide anion (Figure 11a) at all temperatures is important. The $U_{parallel}$ (O4) values correspond to root-mean-square displacements of the order of 0.11 Å, the effect being larger at 50 K than at 5 K or room temperature. This enhanced $U_{parallel}$ of the oxide anions most strongly involved in the Q_2 mode responsible for the ferromagnetic sheets in $LaMnO_3$ is consistent with the presence of incoherent static Q_2 distortions in La_2GaMnO_6. Together with the development of nonzero coherent static Q_2 distortions below the Curie temperature this argues for the importance of this mode in determining the magnetic ordering. An upper bound on the size of the incoherent Q_2 can be estimated by assigning the difference between the

(18) Feinberg, D.; Germain, P.; Grilli, M.; Seibold, G. *Phys. Rev. B* **1998**, *57*, R5583−R5586.

(19) Rodriguez-Carvajal, J.; Hennion, M.; Moussa, F.; Moudden, A. H.; Pinsard, L.; Revcolevschi, A. *Phys. Rev. B* **1998**, *57*, R3189−R3192.

(20) Reinen, D.; Friebel, C. *Struct. Bonding* **1979**, *37*.

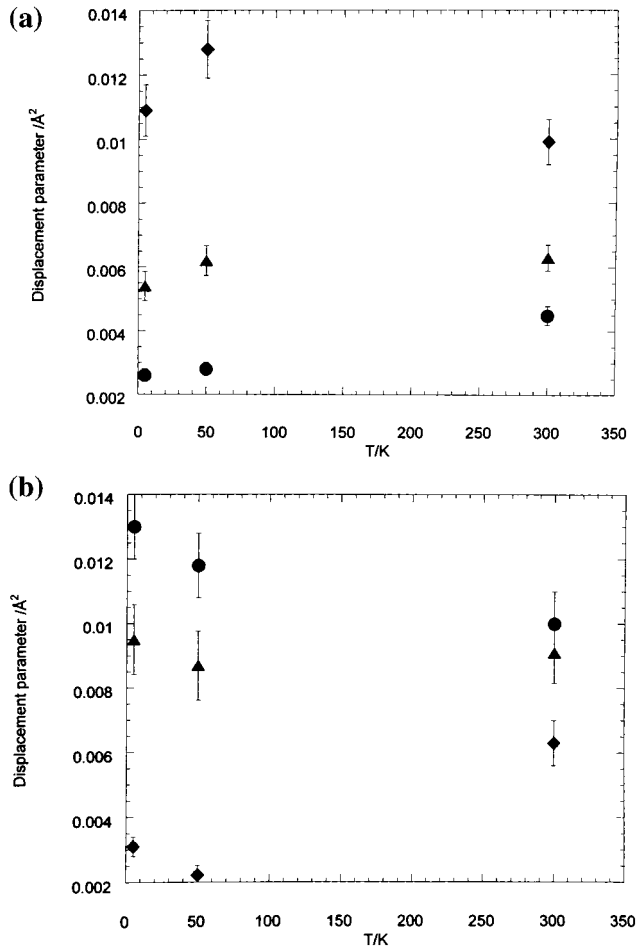

Figure 11. Temperature dependence of the components of the anisotropic displacement parameters of the oxide anions in La_2GaMnO_6 parallel and perpendicular to the Mn−O bonds. Displacements perpendicular to the Mn−O bond are represented as circles, parallel displacements as diamonds, and the equivalent isotropic displacement parameters as triangles. (a) Parameters of the O4 anion. (b) Parameters of the O5 anion.

long and short Mn−O bonds in the *xy* plane as $2\sqrt{U_{11}(O4)}$ yielding $Q_2^{\text{incoherent}} = 0.32(1)$ at 50 K, comparable with $Q_2^{\text{incoherent}} = 0.383$ in $LaMnO_3$ and an order of magnitude larger than the static coherent Q_2 and Q_1 distortions in La_2GaMnO_6. This estimate is an upper bound because there will be a contribution to the static oxide disorder due to the size difference between Ga^{3+} and Mn^{3+}. This shows the importance of considering the incoherent displacements when the static coherent Jahn−Teller distortions are small. The unusual shape of the O5 ellipsoid in La_2GaMnO_6 is further evidence for the importance of static disorder in this material.

Although the Q_2 mode as a common feature of $LaMnO_3$ and La_2GaMnO_6 explains the existence of ferromagnetic sheets in the *ac* plane of the magnetic structure of La_2GaMnO_6, it does not account for the ferromagnetic ordering of those sheets, as opposed to the A-type antiferromagnetism arising from antiferromagnetic coupling of the sheets found in $LaMnO_3$. Recent theoretical work indicates that the precise orbital parentage of the $|a\rangle$ and $|b\rangle$ states strongly controls the sign of the magnetic coupling within and between the planes, with the F or A-type AF ground states arising from different values of Q_2/Q_1.[18] It is thus possible that the combination of incoherent and coherent static Jahn−Teller distortions place La_2GaMnO_6 in the ferromagnetic part of this phase diagram. Ferromagnetic order requires both $Q_2/|Q_1| < 2.6$ and that Q_1 is negative, and so the static incoherent component of Q_1 would have to outweigh the coherent component computed from the bond lengths. An approximate calculation to modify the static coherent Q_1 by the incoherent contribution by adding the rms displacement parallel to Mn−O(4) to both bonds in the *xy* plane yields $Q_1^{\text{incoherent}} = -0.17(4)$ and $Q_2/|Q_1| = 1.9(4)$ which lies within the required range for ferromagnetic rather than A-type antiferromagnetic order. This addition of incoherent to coherent components of the Jahn−Teller distortion at the Mn^{III} centers in La_2GaMnO_6 yields a total local distortion measured by $\sqrt{Q_1^2 + Q_2^2}$ of 0.36(2), which is comparable with the static distortion in $LaMnO_3$. This agreement of the local Jahn−Teller energy at the Mn^{III} sites in the dilute and parent phases suggests that assigning the O4 rms displacement parallel to the Mn−O4 bond to a static incoherent Jahn−Teller distortion is correct. It should be noted that the significant tilting of the BO_6 units places a strong restriction on the extent to which 180° superexchange arguments can be used, although the tilt angles are similar in $LaMnO_3$ and La_2GaMnO_6.

The 5 K zero-field moment per Mn of La_2GaMnO_6 is considerably reduced from the spin-only value of $4\mu_B$. 50% nonmagnetic dilution of the B-site of a perovskite leaves 85% of the B sites connected to a magnetic backbone,[21] so a reduction to 3.4 μ_B per Mn might be expected, but the observed value of 2.80(5) μ_B is surprisingly low. As in this case the exchange interactions arise from specific correlated orbital orderings at neighboring Mn sites, dilution would be expected to have a more significant effect on the moment than in a perovskite where orbital ordering is unimportant. Evidence in favor of the ferromagnetic moment in La_2GaMnO_6 being reduced in zero-field by varying local environments is provided by the larger value of the saturation moment seen at 2 T in the 5 K magnetization isotherm than in the zero-field powder neutron diffraction refinements. The observation of a paramagnetic moment greater than the spin-only value at temperatures above T_c suggests that spin clusters develop in the high-temperature region.

The above arguments rely on σ superexchange between localized Mn^{III} centers alone to explain the observed ferromagnetism of La_2GaMnO_6. The transport and magnetotransport data are consistent with the composition refined from the multihistogram analysis of diffraction data as they indicate that La_2GaMnO_6 is an insulator, suggesting that Mn is entirely in the +III oxidation state. This produces a large Mott−Hubbard barrier to charge transport between the Mn^{III} sites, and therefore arguments based on e_g delocalization to form magnetic polarons or other double exchange related ideas do not apply. Thermopower measurements find a small number of p-type carriers in samples of composition $La_2GaMnO_{6.00\pm0.02}$.[3] Ferromagnetism and magnetoresistance of up to 40% can be observed in B-site substituted manganates ($La_{1.5}Sr_{0.5}RhMnO_6$) in which carriers have been introduced into the e_g orbitals by oxidation.[22]

The magnetic behavior of Nd_2GaMnO_6 at 5 K appears intermediate between that of $LaMnO_3$ and La_2GaMnO_6, with the ferromagnetic sheets common to both being coupled both ferromagnetically and antiferromagnetically along the *b* axis. The extent of the static Jahn−Teller distortion coherent with the *Pnma* symmetry is much greater in Nd_2GaMnO_6 than in La_2GaMnO_6. This may be attributed in part to a synergic interaction between the static distortion in $NdMnO_3$ of Jahn−Teller origin[16] and the unexpectedly large departure from regular

(21) Gibb, T. C. *J. Mater. Chemi.* **1992**, *2*, 415.

(22) Bakowski, B.; Battle, P. D.; Cussen, E. J.; Noailles, L. D.; Rosseinsky, M. J.; Coldea, A. I.; Singleton, J. *Chem. Commun.* **1999**, 2209.

octahedral geometry at the B site in $NdGaO_3$.[14] This allows significant cooperative distortion at neighboring Ga and Mn centers: the Ga center is able to accommodate the distortion required by a neighboring Mn^{III} site. The total coherent distortion measured by $\sqrt{(Q_1^2 + Q_2^2)}$ is 0.237(2) at 5 K (compared with 0.253 predicted from 50% dilution of $NdMnO_3$ by $NdGaO_3$), suggesting that a smaller part of the local E_{JT} is attributable to the incoherent distortions represented by the displacement parameter ellipsoids than is the case for La_2GaMnO_6. The values of Q_2 (= 0.222(2)) and Q_1 (=−0.083(1)) create competition between ferromagnetic and antiferromagnetic coupling along the *b* axis according to the theory of ref 18, although the marked nonlinearity of the superexchange pathways is an additional factor to be considered. The value of $Q_2/|Q_1|$ (2.67(4)) at 5 K is close to the ratio for crossover between ferromagnetic and antiferromagnetic coupling estimated at 2.6. The proximity to this crossover point combined with the variation in local Mn environment due to the disordered Ga^{3+} substitution may then account for the observation of both ferromagnetic and antiferromagnetic coupling along the *b* axis.

The large static coherent Q_2 distortion will give rise to orbital ordering producing the half-filled/empty orbital superexchange, which in turn creates the ferromagnetic sheets in the *ac* plane of the magnetic structure. The observed static coherent distortions are thus consistent qualitatively with the observed complex magnetic structure in which the ferromagnetic sheets are coupled both ferromagnetically and antiferromagnetically along *b*. In contrast to La_2GaMnO_6, the Q_2 distortion is slightly reduced from its room temperature value of 0.233 on cooling through the magnetic ordering temperature. The evolution of this distortion across the other magnetic transition suggested by the $d\chi/dT$ curve will be of interest. The static coherent $Q_2/|Q_1|$ ratio is similar to $LaMnO_3$ but the significance of the incoherent static and dynamic displacements should not be neglected in this case. The oxide displacement parameter ellipsoids in Nd_2GaMnO_6 have more conventional shapes than those found in the lanthanum analogue but both increase on cooling from 300 to 5 K and are larger than those in $LaMnO_3$, suggesting that incoherent contributions may still be important in determining $Q_2/|Q_1|$ locally. Differences in the absorption treatment applied to the 300 and 5 K data for this phase should be borne in mind when comparing the displacement parameters. However, the comparison of HRPD 5 K and HRPD 300 K refinements shows that the ellipsoids determined by time-of-flight diffraction are correct. The role of coupling to the Nd sublattice at low temperature and the evidence for other magnetic ordering transitions between 5 and 300 K (Figure 9b) suggests that a detailed study of the temperature and field dependence of the crystal and magnetic structures of this material should be performed.

The total ordered magnetic moment per Mn^{3+} in zero field in Nd_2GaMnO_6 at 5 K is 2.8(1) μ_B and that of Nd^{3+} is 1.06(6) μ_B. The latter value is in reasonable agreement with that found (1.3 μ_B) in $NdCrO_3$ at 4.2 K.[13] The refined Mn moment agrees precisely with that in the 50% site-diluted ferromagnet La_2GaMnO_6, suggesting that in both cases the origin of the reduction is in the random distribution of Mn^{3+} and Ga^{3+} over the octahedral sites of the lattice. The coupling along the [010] direction of the unit cell indicates that competing superexchange interactions are present in this material. In the case of a perfectly ordered compound this would lead to an identical, canted, moment on each Mn site. However, in the system under discussion the random distribution of Mn^{3+} and Ga^{3+} results in octahedral sites having a range of magnetic environments, depending on the ions occupying the neighboring sites. The orientation of the magnetic moment for a given site may therefore depart from the average direction observed by neutron diffraction.

The measurement of magnetization as a function of field performed at 5 K has given a value for the maximum value for the magnetic moment of 6.08(3) μ_B per Nd_2GaMnO_6 unit. This is greater than the ferromagnetic moment (4.5(2) μ_B) extracted from the D2b neutron diffraction data collected at 5 K in zero field. This suggests that the application of a large field will increase the extent of ferromagnetic coupling at the expense of the antiferromagnetic component of the Mn^{3+} ordering. It is likely that this is responsible for the disparity between these two values for the ordered moment.

In both the magnetometry and neutron diffraction data the maximum observed ordered moment is less than might be expected; the ordered magnetic moment of Nd^{3+} has been observed[12] to be as large as 1.6 μ_B, and if this value was achieved in Nd_2GaMnO_6 a maximum ordered moment of 7.2 μ_B per formula unit would arise. It is therefore clear that at 5 K after cooling the sample in a measuring field of 50 kOe not all of the moments are aligned in the direction of the applied field. While randomly orientated domains lead to zero bulk magnetization, and a small domain size could lead to a reduction in the value observed by a neutron diffraction experiment, neither of these effects would be expected to reduce the magnetization from the saturated value after field cooling the sample from the paramagnetic regime. We thus conclude that the reduction in the ordered magnetic moment observed in both the magnetometry experiments and neutron diffraction data are symptomatic of disruption to the magnetic structure due to the random distribution of Mn^{3+} and Ga^{3+} over the octahedrally coordinated sites introducing variations in the local magnetic environment.

The Curie−Weiss fit to the magnetic susceptibility data shows that the sample is paramagnetic in the range fitted ($175 \leq T/K \leq 300$), giving a value for the paramagnetic moment of 6.70(2) μ_B per Nd_2GaMnO_6. This is in reasonable agreement with the theoretical value of 7.08 μ_B predicted by assuming the orbital contribution is present from Nd^{3+} (3.62 μ_B) and fully quenched in the case of Mn^{3+} (4.90 μ_B). The data show reasonable agreement with the Curie−Weiss law for $T \geq 80$ K and both the field-cooled and the zero-field-cooled susceptibilities clearly increase above the paramagnetic values below the Curie temperature of ca. 40(5) K in excellent agreement with the value for the Weiss constant of 45.9(4) K further confirming the validity of the Curie−Weiss fit carried out to the high-temperature region. Below 21(1) K the field-cooled and zero-field-cooled data diverge and the latter passes through a maximum value at 14(1) K. Consideration of these data in conjunction with the information extracted from the neutron diffraction data led us to conclude that either or both of the Nd^{3+} or Mn^{3+} sublattices order with a net magnetization at 40(5) K. It is probable that the maximum in the susceptibility data observed at 14(1) K is associated with the elimination of the antiferromagnetic component of the Mn^{3+} ordering which was observed by neutron diffraction in zero field at 5 K. The determination of Q_2 and Q_1 as a function of temperature in this range will be important.

We have taken great care to ensure that sample **B** of Nd_2GaMnO_6 is a single-phase material. Although diffraction data from sample **A** have been fitted sufficiently well that the criteria normally applied to characterization by powder diffraction have been satisfied, we believe this sample cannot usefully be described as a single phase. The change in lattice parameters

and the variation in the peak shape of the 200 reflections between the air-cooled sample **A** and N_2-quenched sample **B** show that Nd_2GaMnO_6 undergoes a structural transition on cooling from 1400 °C to ambient temperature. The nature of the low-temperature phase present in sample **A** is unknown. The difference between the two components of that sample may arise in the microstructure, rather than in the crystal structure.

Conclusion

Substitution of Ga^{3+} into the octahedral site of $LnMnO_3$ (Ln = La, Nd) phases results in the retention of the ferromagnetic sheets found in A-type $LaMnO_3$, but the pronounced influence of the spherical cation on the static coherent Jahn−Teller distortion in $LaMnO_3$ results in total (La) or partial (Nd) ferromagnetic coupling of these sheets. In La_2GaMnO_6 a small static Q_2 distortion develops below T_c, consistent with the planar ferromagnetic coupling, but the size of the static coherent distortion is too small to account for the significant Jahn−Teller splittings which must be present locally at individual Mn^{III} sites. The static incoherent displacements evident from the shape, size, and temperature dependence of the oxide displacement parameters allow the inference of local Q_2 and Q_1 modes of size and sign consistent with ferromagnetism[18] and of total (coherent plus incoherent) magnitude consistent with local distortions comparable in size with those in $LaMnO_3$. The magnetic structure of Nd_2GaMnO_6 has an A-type antiferromagnetic component similar to $LaMnO_3$ but also ferromagnetic coupling similar to La_2GaMnO_6. The static coherent Jahn−Teller distortion here is over an order of magnitude larger than that in La_2GaMnO_6, and is of the type giving ferromagnetic planes via orbital-ordering controlled superexchange. The Q_2/Q_1 ratio places the material close to the predicted crossover between ferromagnetic and A-type antiferromagnetic ordering. The role of static incoherent distortions could still be significant as the displacements of both crystallographically distinct oxide anions parallel to the Mn−O bonds increase on cooling. There are higher temperature magnetic ordering transitions in Nd_2GaMnO_6 evident from magnetization measurements.

Acknowledgment. We are grateful to Dr. T. Hansen at the ILL, Grenoble and to Dr. R. M. Ibberson at Rutherford−Appleton Laboratories, Oxon for experimental assistance with the neutron diffraction experiments, and the UK Engineering and Physical Science Research Council for funding.

Supporting Information Available: Figure showing Rietveld refinement of neutron diffraction data collected at 5 K on sample A of Nd_2GaMnO_6 as a single phase and as a biphasic mixture (PDF). This material is available free of charge via the Internet at http://pubs.acs.org.

JA003139I